

# **Mechanical Properties of Short-fibre Layered Composites**

**G. Zak\*, C. B. Park<sup>†</sup>, B. Benhabib<sup>†</sup>**

**\*Department of Mechanical Engineering**

**Queen's University, Kingston, Ontario, Canada K7L 3N6**

**<sup>†</sup>Computer Integrated Manufacturing Laboratory**

**Department of Mechanical and Industrial Engineering**

**University of Toronto, Toronto, Ontario, Canada M5S 3G8**

## **Abstract**

Recent research work has explored the use of glass fibre reinforcements for improvement of the mechanical properties of polymer-based parts produced by Layered Manufacturing (LM) techniques. In this paper, a model based on the modified rule-of-mixtures is employed for the mechanical-property prediction of short-fibre-reinforced photo-sensitive polymers produced by the layered manufacturing process developed by the authors. The predictions employ the empirical data collected on the fibre-matrix interface, the fibre geometrical arrangement within the specimens, and the fibre length. The fibre geometrical arrangement is characterized by the fibre-orientation distribution, while the fibre length is characterized by the fibre-length distribution. The effect of fibre orientation and length is accounted for in the model by the fibre-length correction and orientation-efficiency factors. Comparison of actual observations and predictions of mechanical properties of layered composites demonstrated the effectiveness of the proposed methodology.

April 1999

## 1 Introduction

Reinforcement of plastics by short fibres has been employed successfully as means of improving the mechanical properties of the manufactured products. Recent research work has targeted improvement of the mechanical properties of polymer-based parts produced by Layered Manufacturing (LM) techniques utilizing long and short fibres and even microspheres. Most pertinent to this paper, in Ogale et al., 1991, and in Renault and Ogale, 1992, composite samples several-layers thick were produced by manually spreading short glass fibres over the photo-sensitive liquid resin on each layer. Improvements of material mechanical properties were reported for fibre-based reinforcements, while no improvement was attained by using microspheres. For the LM process proposed in Zak et al., 1996, significant improvements in the tensile modulus of the layered parts were also reported.

There exists a number of models for predicting composite-material properties. For example, the Mori-Tanaka theory (Mori and Tanaka, 1973) evaluates the average internal stress in the matrix of a material with ellipsoidal inclusions. While the theory requires knowledge of the shape and orientation of every particle, in practice, statistical descriptions in the form of the fibre-orientation and fibre-length distributions are used. Both Pettermann et al., 1997, and Biolzi et al., 1994, use the generalized Mori-Tanaka mean-field approach to take into account the fibre-orientation distribution (FOD) and thus predict modulus and strength of short-fibre composites. Fu and Lauke, 1996, predict the tensile strength of short-fibre composites using the modified rule-of-mixtures expression and by calculating the product of the fibre-length and orientation-correction factors as a function of the FOD and fibre-length distribution (FLD).

In this paper, the most commonly used and comparatively straightforward model based on the modified rule-of-mixtures expression is employed for the mechanical-property prediction of short-fibre-reinforced photo-sensitive polymers produced by the layered manufacturing process described in Zak et al., 1996. This model is used to predict the mechanical properties of layered parts based on the information obtained a priori on the fibre-matrix interface and on the fibre geometrical arrangement.

## 2 RLCM Process

The primary fabrication steps of our rapid layered composite manufacturing (RLCM) process are as follows, Figure 1:

- (1) A precise volume of a composite liquid (resin and short fibres) is withdrawn from an external source and deposited from above for each layer (Figure 1 (a));
- (2) The liquid is levelled at the required height by a straight-edge blade (Figure 1(b));
- (3) The layer is selectively cured by a UV laser, in a way which allows interlayer crossing of fibres (Figure 1(c)); and,
- (4) A platform supporting the part is lowered by one layer (Figure 1(d)).

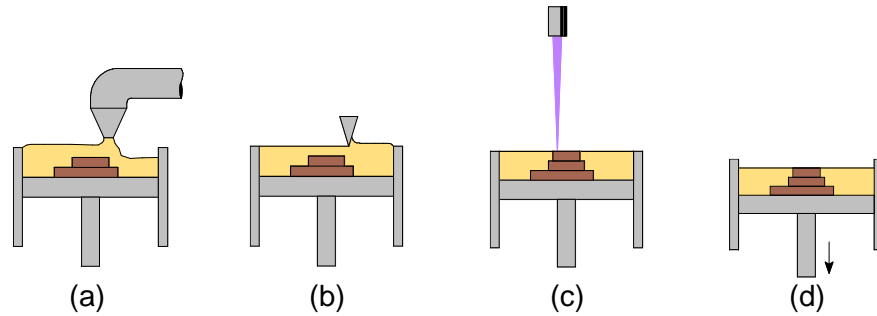


**Figure 1. Steps of the proposed RLCM process.**

The process steps are repeated until the entire part is built. Subsequently, the platform is raised, and the part is removed, cleaned, and post-cured. As the fabrication process continues, the composite liquid is continuously mixed in a separate container, i.e., an external raw-material source.

A novel aspect incorporated into the proposed process is the creation of *interlayer bonding sites*. Since the liquid surface tension would keep the fibres from protruding above the surface, with the normally performed complete-surface solidification, there would be no fibres crossing the layer boundaries. The proposed bonding sites are formed by using a special X-Y laser-scanning pattern that leaves small volumes of resin uncured within each layer (Figure 2). Fibres protrude into these volumes from the surrounding solidified resin. When the subsequent layer is spread and cured, it extends into the uncured pockets left in the preceding layer and forms an interlayer bonding site. The site locations alternate from layer to layer. Figure 3 attempts to illustrate this concept graphically. It shows the sequential formation of three consecutive layers. (The darker shading indicates solidified resin, while the lighter semi-transparent volumes denote uncured liquid.)

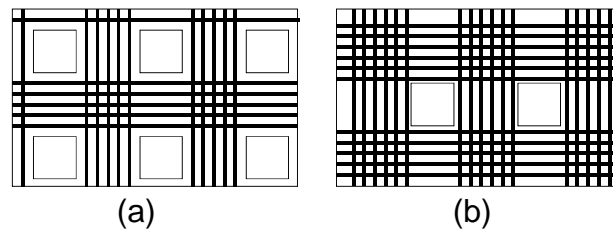


**Figure 2. Scanning patterns that produce the interlayer bonding sites: (a) odd-numbered layer and (b) even-numbered layer (thick lines mark the laser scan paths).**

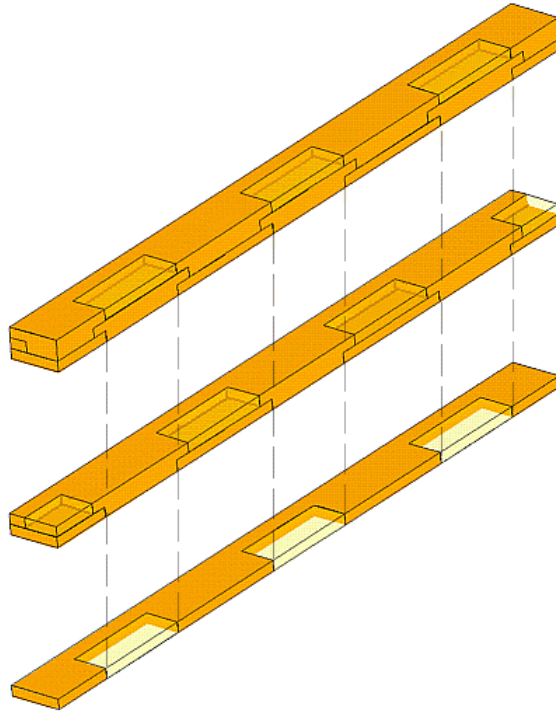


**Figure 3. Schematic illustration of the interlayer bonding sites (half of a cross-section is shown).**

### 3 Estimation of Mechanical Properties

#### 3.1 Modulus Prediction for Aligned Short Fibres

For short fibres, when the composite is stressed, the stresses are transferred to the fibres by shear at the fibre surfaces, which causes the fibres to deform. Since the fibres are much stiffer than the matrix, the fibre strain is smaller than the overall strain in the composite.

To estimate the tensile modulus of a short-fibre composite, Cox, 1952, proposed a theory (later referred to as a “shear-lag” theory) that assumes a completely elastic transfer of stresses from the matrix to the fibre. This analysis considers an ideal case of short fibres aligned with the stress direction and arranged in a particular pattern (e.g., a square or a hexagonal array). The theory derives the distribution of tensile stress within the fibre, along its axial direction. Thus, the stress at distance  $x$  from the fibre centre is given by

$$\sigma_f(x) = E_f \varepsilon_1 \left( 1 - \frac{\cosh(2n_c x / d)}{\cosh(n_c s)} \right), \quad (1)$$

where

$$n_c = \sqrt{\frac{2G_m}{E_f \ln(2R/d)}}, \quad G_m = \frac{E_m}{2(1+\nu_m)}, \quad \frac{2R}{d} = \sqrt{\frac{\pi}{4\nu_f}}, \quad \text{and} \quad s = \frac{l}{d}. \quad (2)$$

Above,  $s$  is the aspect ratio for fibres of length  $l$  and diameter  $d$ ,  $R$  is “fibre-packing” distance,  $G_m$  is the matrix shear modulus,  $\nu_m$  is the matrix Poisson ratio,  $\varepsilon_1$  is the composite strain in the loading direction,  $\sigma_f$  and  $E_f$  are the fibre, and  $\sigma_m$  and  $E_m$  are

the matrix stress and tensile modulus, respectively, and  $v_f$  and  $v_m$  are the fibre and matrix volume fractions, respectively.

By averaging the stress distribution within the fibres, the theory predicts the tensile modulus for aligned short-fibre composites, in the direction of alignment, to be equal to:

$$E_1 = \chi_2 v_f E_f + v_m E_m, \quad (3)$$

where *fibre-length correction factor*,  $\chi_2$ , is equal to:

$$\chi_2 = 1 - \frac{\tanh(n_c s)}{n_c s}. \quad (4)$$

### 3.2 Modulus Prediction Based on Fibre-Orientation Distribution

When fibres are *not* perfectly aligned with the direction of modulus estimate, an *orientation-efficiency factor*,  $\chi_1$ , is added to the Equation (3) (Hull, 1981):

$$E_c = \chi_1 \chi_2 v_f E_f + v_m E_m, \quad 0 < \chi_1 < 1. \quad (5)$$

For in-plane uniformly distributed fibre orientations, the factor is 3/8 when estimating the in-plane composite modulus. The factor is 1/5 for three-dimensional uniform fibre-orientation distribution.

The orientation-efficiency factor can be calculated more accurately, however, if the fibre-orientation distribution (FOD) is known. While in general FOD is a joint probability density function of two angles,  $p(\theta, \phi)$ , for the approach described below, a marginal distribution with respect to angle  $\phi$  only is required,  $p(\phi)$ , (Figure 4). Angle  $\phi$  is defined as the angle between the direction of interest and the fibre axis.

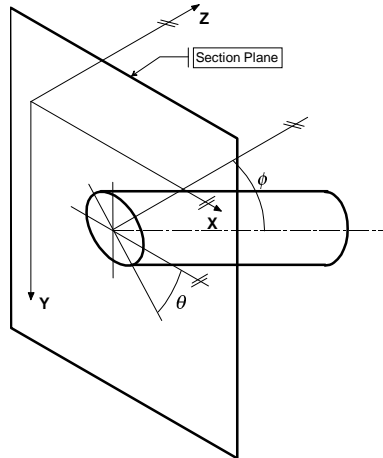


**Figure 4. Fibre orientation angles.**

To estimate the orientation-efficiency factor,  $\chi_1$ , the composite is modelled as a laminate consisting of laminae with different fibre orientations (Sanadi and Piggott, 1985). Each lamina  $k$  is assigned a thickness,  $t_k$ , proportional to the fraction of fibres at this particular angle:

$$t_k = K p(\phi_k). \quad (6)$$

Laminate theory predicts the modulus along the  $Z$  direction for fibres aligned at angle  $\phi$  to  $Z$  as (Jones, 1975):

$$\frac{1}{E_\phi} = \frac{\cos^4 \phi}{E_1} + \left( \frac{1}{G_{12}} - \frac{2\nu_{12}}{E_1} \right) \sin^2 \phi \cos^2 \phi + \frac{\sin^4 \phi}{E_2}. \quad (7)$$

In the above,  $E_1$  is the tensile modulus for perfectly aligned long fibres. Also,  $E_2$ , the composite tensile modulus in the transverse direction,  $G_{12}$ , the composite shear modulus, and  $\nu_{12}$ , the composite Poisson's ratio, are given by:

$$\frac{1}{E_2} = \frac{\nu_f}{E_f} + \frac{\nu_m}{E_m}, \quad \frac{1}{G_{12}} = \frac{\nu_f}{G_f} + \frac{\nu_m}{G_m}, \quad \text{and} \quad \nu_{12} = \nu_f \nu_f + \nu_m \nu_m. \quad (8)$$

Given the relative thickness of each lamina  $k$ ,  $t_k$ , from Equation (6), the value of  $\chi_1$  is estimated by:

$$\chi_1 = \frac{\sum_{k=1}^n E_{\phi k} t_k}{E_1 \sum_{k=1}^n t_k}. \quad (9)$$

### 3.3 Strength Prediction Based on Fibre-Orientation Distribution

Prediction of the tensile strength for short-fibre composites is a difficult task, and no universally accepted theory exists on this subject. The difficulty arises because the material's ultimate strength in the case of composites is determined by the onset of fracture, and not via a yielding mechanism. Composite strength models most frequently take the form of:

$$\sigma_c = \chi_3 \chi_4 \nu_f \sigma_{fu} + \nu_m \sigma_m^*, \quad (10)$$

where  $\sigma_{fu}$  is the fibre tensile strength,  $\sigma_m^*$  is the tensile stress in the matrix at composite failure strain, and  $\chi_3$  and  $\chi_4$  are the fibre-length correction and orientation-efficiency factors, respectively, for composite strength. The difficulty lies in the estimation of the correction factors.

Piggott, 1994, proposes that the short-fibre composite strength model should be derived from a fracture-based, instead of slip-based theory (Kelly, 1973). Thus, Piggott, 1994, gives the fibre-length correction factor as:

$$\chi_4 = \begin{cases} 1 - s_c / 2s - 12.5 / s s_c + 5\sigma_{mu} / s\sigma_{fu} & \text{for } s > s_c, \\ (s / s_c)(1 - 25 / s^2) + 5\sigma_{mu} / s\sigma_{fu} & \text{for } s \leq s_c, \end{cases} \quad (11)$$

where  $\sigma_{mu}$  is the matrix ultimate tensile strength and  $s_c = \sigma_{fu} / 2\tau_{iu}$  is the critical aspect ratio for the composite, with  $\sigma_{fu}$  being the fibre's ultimate tensile strength and  $\tau_{iu}$  being the interfacial shear strength.

To account for fibre misalignment in the strength model, an approach based on the strain-energy concept can be used (Sanadi and Piggott, 1985). The orientation-efficiency factor is calculated by summing contributions from  $n$  "laminae" of

thickness  $t_k$ , with fibres in each lamina oriented at angle  $\phi_k$  and thickness proportionate to the number of fibres oriented at an angle  $\phi_k$ :

$$\chi_3 = \frac{\sum_{k=1}^n \sigma_{u\phi_k} t_k}{\sigma_{1u} \sum_{k=1}^n t_k}, \quad (12)$$

with  $\sigma_{u\phi_k}$  given by

$$\frac{1}{\sigma_{u\phi_k}^2} = \frac{\cos^4 \phi}{\sigma_{1u}^2} + \left( \frac{1}{\tau_{12u}^2} - \frac{1}{\sigma_{1u}^2} \right) \sin^2 \phi \cos^2 \phi + \frac{\sin^4 \phi}{\sigma_{2u}^2}, \quad (13)$$

where

$$\sigma_{1u} = \nu_f \sigma_{fu} + \nu_m \sigma_m^*, \quad \tau_{12u} = \sigma_{mu} / 2, \quad \text{and} \quad \sigma_{2u} = \sigma_{mu}. \quad (14)$$

### 3.4 Accounting for Fibre-Length Distribution

The effect of finite fibre length is accounted for herein by the fibre-length correction factors:  $\chi_2$  for modulus and  $\chi_4$  for strength. When the fibre length is not uniform, the factors can be obtained as weighted sums, with the weights determined by the fibre-length distribution (Piggott et al., 1993). To calculate these weights, the FLD has to be modified to represent *the fraction of the total fibre volume*, as opposed to *the number of fibres*, for each fibre length interval.

Assuming the average fibre diameter is the same for fibres of all lengths, the total volume occupied by fibres in any particular length range is proportional to the number of fibres in that range multiplied by the fibre length. If the probability of finding fibres of length  $l$  is  $p(l)$ , then the weighting factor proportional to the total volume of all length  $l$  fibres is

$$P_s = l p(l). \quad (15)$$

For example, the fibre-length distribution (FLD) represented by a Weibull distribution with  $a=0.1$  and  $b=1.2$  is plotted in Figure 5. The plot shows the length distribution both in terms of a “number fraction,”  $p(l)$ , and in terms of a “volume fraction,”  $P_s$ . Since the longer fibres occupy relatively greater volume than the shorter ones, the  $P_s$  distribution is skewed towards the greater fibre lengths compared with original  $p(l)$  distribution.

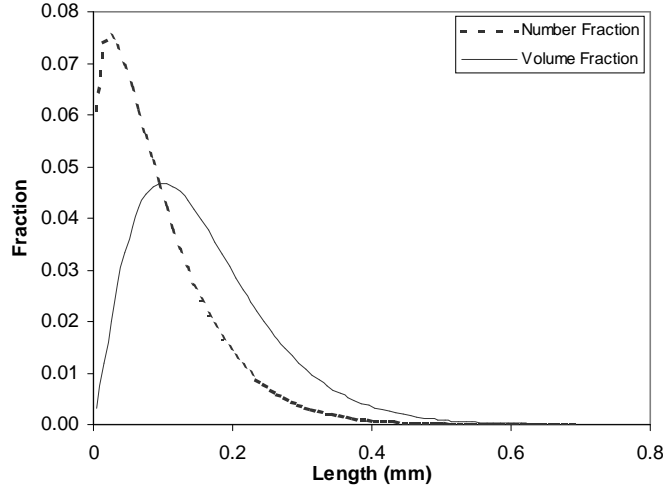


**Figure 5. Fibre-length distribution plotted as “number fraction” and “volume fraction” of the fibres (Weibull distribution with  $a=0.1$  and  $b=1.2$ ).**

Therefore, to account for fibre-length distribution, the fibre-length correction factor for modulus is calculated as (Piggott et al., 1993):

$$\chi_2 = \sum_{k=1}^m P_{sk} \{1 - \tanh(ns_k) / ns_k\}, \quad (16)$$

where  $P_{sk}$  is the fraction of the total fibre volume occupied by fibres with the aspect ratio  $s_k$ .

The fibre-length correction factor for strength is given by (Piggott et al., 1993):

$$\chi_4 = \sum_{k=1}^m P_{slk} \{1 - s_c / 2s_k\} + \sum_{k=1}^m P_{ssk} s_c / 2s_k, \quad (17)$$

where  $P_{slk}$  is the fraction of the total fibre volume occupied by *longer* fibres, having aspect ratio ( $s_k > s_c$ ), and  $P_{ssk}$  is the corresponding fraction occupied by *shorter* fibres, having aspect ratio ( $s_k \leq s_c$ ).

### 3.5 Predictions of Direction-Dependent Mechanical Properties

The material properties of the short-fibre layered composites considered in this paper are a function of direction. The anisotropy is mainly caused by the non-uniformity in spatial distribution of fibre orientations. The fibres have a tendency to align parallel to layer planes. Furthermore, in layered parts, the interlayer boundaries may also weaken the mechanical properties transverse to the layer plane. Therefore, short-fibre layered composites can be described as either (a) orthotropic materials or (b) transversely isotropic materials. Orthotropic materials have three mutually orthogonal planes of symmetry for material properties (Figure 6). Transversely isotropic materials have mechanical properties independent of the direction within the layer plane (normal to Z axis in Figure 6).

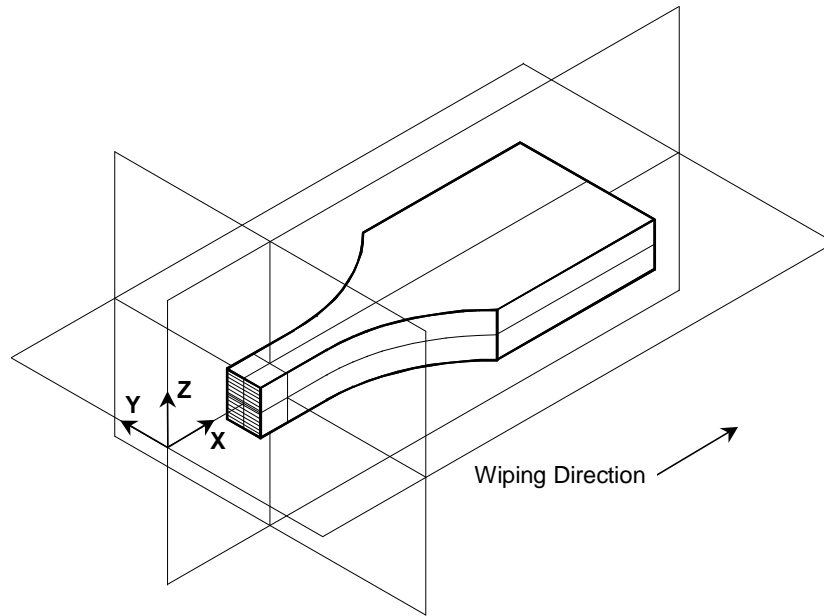


**Figure 6. Principal directions and orthogonal planes of an orthotropic material.**

The direction-dependent tensile moduli and tensile strengths are estimated below for an exemplary layered composite sample. The three principal directions are defined as in Figure 6, where  $X$  is parallel to the wiping direction and  $Z$  is normal to the layer plane. The tensile modulus and strength are estimated in each direction by evaluating Equations (5) and (10), respectively. The fibre-orientation and fibre-length distributions are used to evaluate the orientation-efficiency ( $\chi_1$ ) and fibre-length correction ( $\chi_2$ ) factors, Equations (9), (12), (16) and (17).

The material properties of the constituent components and of their interface are given in Table 1. Tables 2 and 3 show the resulting predictions for modulus and strength along the three principal directions. As can be seen, the orientation particularly impacts the material modulus (by about 30%). An equivalent significant effect on strength is not observed (about 10% variation only). (For comparison purposes, one can note that tensile testing of the specimen under consideration in this section along the  $X$  direction yielded the following results: modulus of 2.43 GPa and strength of 66.9 MPa. The fibre content by volume was measured as 17.9%). More experimental results are provided in Section 4 of this paper.

**Table 1. Constituent component properties used for composite material property predictions.**

Material	Property	Value
Matrix (SL5170)	Tensile modulus, $E_m$ (GPa)	1.37
	Tensile strength, $\sigma_{mu}$ (MPa)	62
	Poisson's Ratio, $\nu_m$	0.35
Fibre (737BD)	Tensile modulus, $E_f$ (GPa)	72
	Tensile strength, $\sigma_{fu}$ (GPa)	3.4
	Poisson's Ratio, $\nu_f$	0.22
Interface	Interfacial shear strength, $\tau_{iu}$ (MPa)	40

**Table 2. Predicted tensile modulus dependence on orientation.**

Direction	Orientation-Efficiency Factor ( $\chi_1$ )	Fibre-Length Correction Factor ( $\chi_2$ )	Predicted Modulus (GPa)
X	0.340	0.291	2.40
Y	0.136	0.291	1.63
Z	0.118	0.291	1.57

**Table 3. Predicted tensile strength dependence on orientation.**

Direction	Orientation-Efficiency Factor ( $\chi_3$ )	Fibre-Length Correction Factor ( $\chi_4$ )	Predicted Strength (MPa)
X	0.191	0.105	63.4
Y	0.098	0.105	57.4
Z	0.091	0.105	57.0

## 4 Model-Based Predictions versus Experimental Results

### 4.1 Tensile tests

Tensile tests were conducted on dogbone-shaped specimens built on the RLCM prototype system, Figure 7. The specimens were tested in tension until failure, with the main parameters observed being the tensile modulus and strength. The composite specimens were fabricated by adding 737BD 1.6-mm glass fibres to SL5170 resin (Ciba-Geigy). The tests reported herein were performed on two sets of four specimens each (Figure 8) – one set with Large and another with Small Interlayer Bonding sites (abbreviated as LIB and SIB sets, respectively). The specimens contained thirteen layers each. The processing parameters were as follows: laser power of 13-15 mW, scan speed of 15 mm/s, and scan line spacing of 0.3 mm. After layered fabrication, the parts were post-cured for two hours using an ultraviolet lamp. Fibre content of the composite specimens was measured via ASTM Standard Test Method D792-91 using water displacement technique.

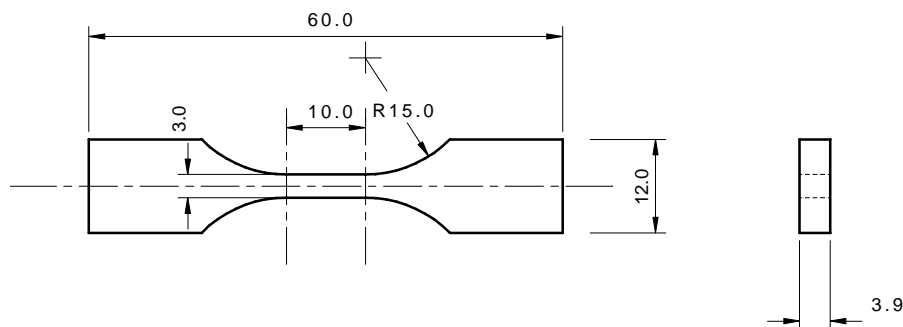


**Figure 7. Dogbone-shaped tensile test specimen (all dimensions are in mm).**

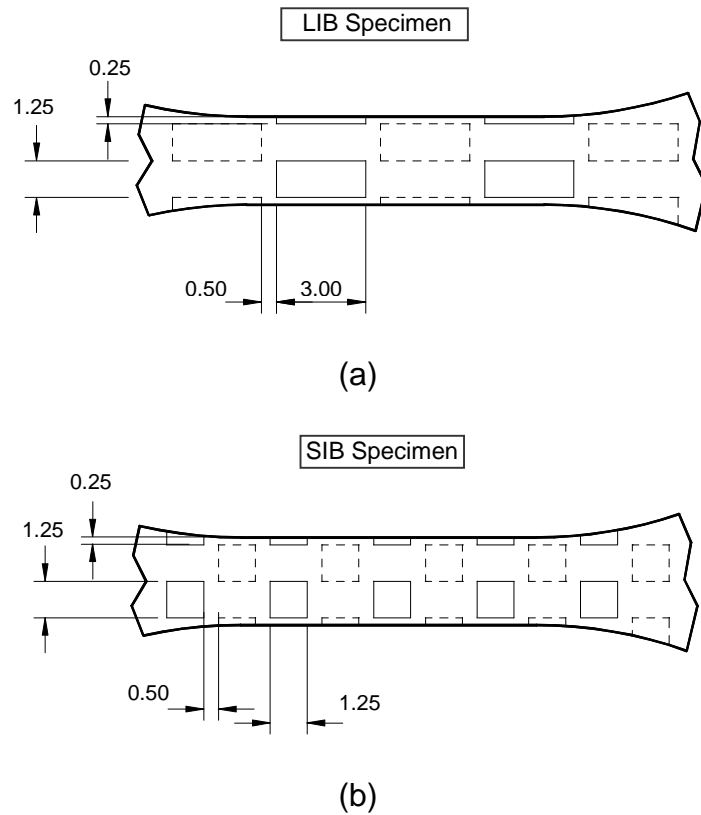


**Figure 8. Interlayer bonding sites within (a) LIB and (b) SIB dogbone specimens. Bonding sites from two consecutive layers can be distinguished by solid and dashed lines. (All dimensions in mm.)**

The tensile testing equipment was Sintech 20 (S/N 657200) with a 500-kg loadcell (Model 3132-149, S/N 10625). The cross-head speed was set to 1 mm/min, as recommended by the ASTM test method specifications. The load vs. extension data were collected using the proprietary digital data acquisition hardware and software.

Fibre content and mechanical property observations for each set are shown in Table 4. (For comparison purposes, layered dogbone specimens with pure resin content and with interlayer bonding were also fabricated and tested. They yielded an average modulus value of 1.42 GPa and an average strength value of 61.9 MPa).

**Table 4. Tensile test results for layered composites.**

Set	Fiber Content (%)		Modulus (GPa)		Strength (MPa)		Strain at Break (%)	
	Ave.	St. Dev.	Ave.	St. Dev.	Ave.	St Dev.	Ave.	St Dev.
LIB	16.0	0.4	2.48	0.10	71.8	1.4	5.3	0.2
SIB	17.0	1.1	2.49	0.19	72.0	4.4	4.8	0.4

## 4.2 Mechanical Property Predictions

The mechanical-property prediction method discussed in Section 3 was applied to predict the modulus and strength values for the composite specimens discussed in Section 4.1 above. The cross-sectional examination of these specimens supplied

us with the necessary information about their microstructure in the form of the fibre-length and fibre-orientation distributions. Since the cross-sectional examination was conducted for only *one specimen* from each set, the predictions were compared with the results obtained for *that particular specimen*.

Table 5 shows the predicted modulus values together with the length and orientation correction factors used to predict them. The predictions and experimental observations are displayed for comparison in Figure 9(a). (The error bars are the standard deviation for the specimens' experimentally observed set of values). As seen, predictions match observations fairly well (within 10%) for both sets of specimens (LIB and SIB).

Table 6 shows the predicted strength values, as well as the correction factors used to obtain them. Figure 9(b) displays the strength predictions and observations (with the error bars from the corresponding sets). Once again, predictions match observations fairly well for both sets of specimens.

**Table 5. Predicted tensile modulus.**

Specimen Set Name	Orientation-Efficiency Factor ( $\chi_1$ )	Fibre-Length Correction Factor ( $\chi_2$ )	Predicted Modulus (GPa)	Observed Modulus (GPa)
LIB	0.266	0.365	2.29	2.46
SIB	0.340	0.291	2.40	2.43

**Table 6. Predicted tensile strength.**

Name	Orientation-Efficiency Factor ( $\chi_3$ )	Fibre-Length Correction Factor ( $\chi_4$ )	Predicted Strength (MPa)	Observed Strength (Mpa)
LIB	0.157	0.138	64.1	72.1
SIB	0.191	0.105	63.4	66.9

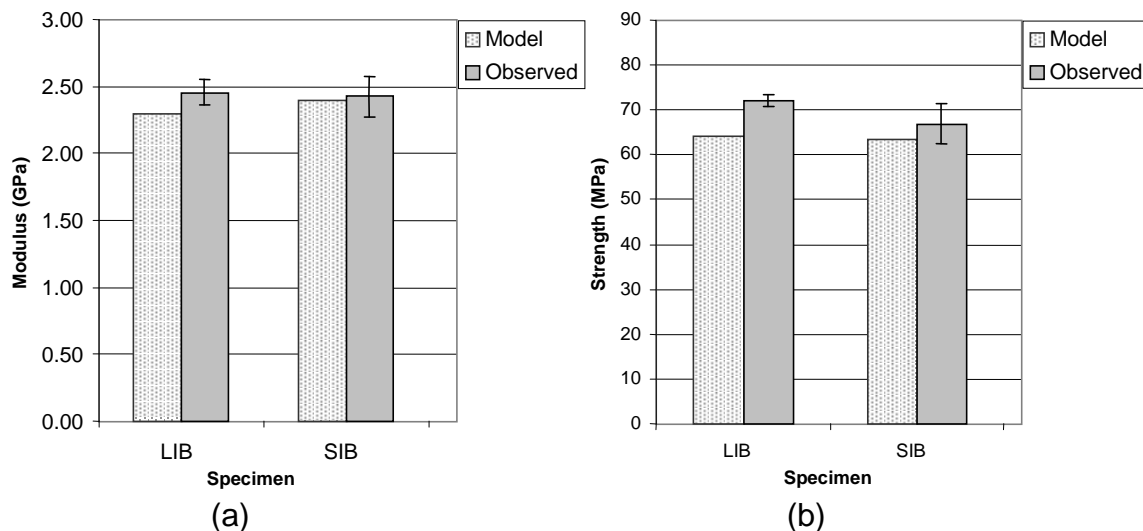


**Figure 9. Comparison of (a) modulus and (b) strength predictions and observations.**

## 5 Conclusions

This paper proposed the use of a modified rule-of-mixtures model to predict the mechanical properties of short-fibre layered composites. The model relies on the fibre-length correction and orientation-efficiency factors to account for the misalignment of fibres with respect to the loading direction. Both factors are to be estimated using the fibre-orientation and fibre-length distributions of the specimens. Comparison of actual observations and predictions of mechanical properties of layered composites demonstrated the effectiveness of the proposed methodology.

## 6 References

- Biolzi, L., Castellani, L., and Pitacco, I., 1994, "On the mechanical response of short fibre reinforced polymer composites," *Journal of Materials Science*, Vol. 29, pp. 2507-2512.
- Cox, H. L., 1952, "The elasticity and strength of paper and other fibrous materials," *British Journal of Applied Physics*, Vol. 3, pp. 72-79.
- Fu, S.-Y., and Lauke, B., 1996, "Effects of fibre length and fibre orientation distributions on the tensile strength of short-fibre-reinforced polymers," *Composites Science and Technology*, Vol. 56, pp. 1179-1190.
- Hull, D., 1981, **An Introduction to Composite Materials**, Cambridge University Press, London.
- Jones, R. M., 1975, **Mechanics of Composite Materials**, McGraw-Hill, New York.
- Kelly, A., 1973, **Strong Solids**, (2<sup>nd</sup> edition), Oxford University Press, Oxford.
- Mori, T., and Tanaka, K., 1973, "Average stress in the matrix and average elastic energy of materials with misfitting inclusions," *Acta Metallurgica*, Vol. 21, pp. 571-574.
- Ogale, A. A., Renault, T., Dooley, R. L., Bagchi, A., Jara-Almonte, C. C., 1991, "3-D photolithography for composite development: discontinuous reinforcements," *SAMPE Quarterly*, October Issue, pp. 28-38.
- Pettermann, H. E., Bohm, H. J., and Rammerstorfer, F. G., 1997, "Some direction-dependent properties of matrix-inclusion type composites with given reinforcement orientation distributions," *Composites Part B*, Vol. 28B, pp. 253-265.
- Piggott, M. R., Ko, M., and Chuang, H. Y., 1993, "Aligned short-fibre reinforced thermosets: Experiments and analysis lend little support for established theory," *Composites Science and Technology*, Vol. 48, pp. 291-299.
- Piggott, M. R., 1994, "Short fibre polymer composites: a fracture-based theory of fibre reinforcement," *Journal of Composite Materials*, Vol. 28, No. 7, pp. 588-606.
- Renault, T., and Ogale, A. A., 1992, "3-D photolithography: mechanical properties of glass and quartz fibre composites," *Proceedings of ANTEC'92 – Conference of SPE*, Vol. 1, pp. 745-747.
- Sanadi, A. R., and Piggott, M. R., 1985, "Interfacial effects in carbon-epoxies: Part 1, Strength and modulus with short aligned fibres," *Journal of Materials Science*, Vol. 20, pp. 421-430.
- Zak, G., Sela, N. M., Park, C. B., Benhabib, B., 1996, "A stereolithography method for the rapid manufacture of glass-fiber-reinforced composites," *ASME International Mechanical Engineering Congress and Exposition*, Atlanta, Georgia, DE-Vol.89, pp. 29-36, November 1996.